Ratchet effect in an asymmetric two-dimensional system of Janus particles

Pavol Kalinay[1] and František Slanina[2]
[1]*Institute of Physics, Slovak Academy of Sciences, Dúbravska cesta 9, 84511, Bratislava, Slovakia*
[2]*Institute of Physics, Czech Academy of Sciences, Na Slovance 2, CZ-18200, Praha, Czech Republic*

(Received 17 March 2023; accepted 28 June 2023; published 25 July 2023)

We consider a disk-like Janus particle self-driven by a force of constant magnitude f, but an arbitrary direction depending on the stochastic rotation of the disk. The particle diffuses in a two-dimensional channel of varying width $2h(x)$. We applied the procedure mapping the $2+1$-dimensional Fokker-Planck equation onto the longitudinal coordinate x; the result is the Fick-Jacobs equation extended by the spatially dependent effective diffusion constant $D(x)$ and an additional effective potential $-\gamma(x)$, derived recursively within the mapping procedure. Unlike the entropic potential $\sim \ln h(x)$, $\gamma(x)$ becomes an increasing or decreasing function also in periodic channels, depending on the asymmetry of $h(x)$ and thus it visualizes the net force driving the ratchet current. We demonstrate the appearance of the ratchet effect on a trial asymmetric channel; our theory is verified by a numerical solution of the corresponding Fokker-Planck equation. Isotropic driving force f results in the monotonic decrease of the ratchet current with a growing ratio $\alpha = D_R/D_T$ of the rotation and the translation diffusion constants; asymptotically going $\sim 1/\alpha^2$. If we allow anisotropy of the force, we can observe the current reversal depending on α.

DOI: 10.1103/PhysRevE.108.014606

I. INTRODUCTION

Active particles [1,2] represent an intriguing realm of nonequilibrium many-particle phenomena. In spite of superficial similarity to ensembles of particles driven by thermal noise, ensembles of active particles exhibit features forbidden by fundamental laws of equilibrium thermodynamics [3–5], due to inherent openness and steady input of energy. A paradigmatic example of experimental realization are Janus particles [6,7] which can be modeled as tiny spheres moving in a viscous environment under the influence of a force, direction of which randomly fluctuates, while its absolute value remains constant.

The tricky behavior of active matter in unbounded space becomes even more subtle when it is confined by a complex geometry [8,9]. Indeed, in the ensembles well known from the equilibrium statistical mechanics, the boundary conditions become irrelevant in the thermodynamic limit (with provision of critical phenomena and phase coexistence). On the contrary, the state of the ensemble of active particles is fundamentally determined by the geometry of the area they are confined to. Indeed, active particles within a container generically accumulate close to the walls. If we look at the mass transport by the particles, boundary currents can dominate over the bulk contribution. Hence, the geometry of the boundaries is essential.

Here, we will study the active Janus particles in quasi-one-dimensional pore with modulated profile. Various modifications of such setup were investigated experimentally [10–18]. From the theoretical side, such systems were already amply studied by numerical simulations [19–28], but analytical results are scarce [21,29].

Here, we aim at a concise analytical description based on projection techniques, namely using the dimensional reduction along the lines of Fick-Jacobs (FJ) approach. This methodology was already successfully used for active particles in channels [30–35], but we will push the method further by projecting out not just the transverse, but also angular degrees of freedom, as done in the simplified setups [36–38]. As mentioned above, the active particles tend to accumulate at walls and this feature represents a challenge for the mapping technique, which enables us to reach a nontrivial result in the higher-order corrections to the basic FJ approximation. Indeed, we will show that including higher order terms is essential in order to grasp the nature of the active particles.

For simplicity we will work in a two-dimensional (2D) space. The generalization to the truly three-dimensional case brings a few difficulties, which are, however, of rather technical and not fundamental nature. We consider here a Janus particle placed in a 2D channel of width $2h(x)$ varying along the longitudinal coordinate x. The particle is represented by a disk of radius $R \ll h(x)$ rotating stochastically, characterized by the rotational diffusion constant D_R. Aside from the (translational) diffusion inside the channel with the diffusion constant D_T, it is self-driven by the force of a constant magnitude f, acting in a direction depending on the angle position ϕ of the active spot on the disk. Recently, several simplified models were solved [36–38], where mainly orientation of the force was reduced either only to the longitudinal or to the transverse directions. Combining the techniques developed in these specific cases enables us to study the dynamics of the true Janus particle driven in an arbitrary direction.

Our study is based on a mapping of the Fokker-Planck equation in two spatial coordinates and the angle ϕ describing the system onto the longitudinal coordinate x. The result is the

generalized FJ equation [39–41],

$$\partial_t p(x,t) = \partial_x A(x) D(x) \partial_x \frac{p(x,t)}{A(x)}, \tag{1.1}$$

governing the marginal probability density $p(x,t)$ of particles along the channel. Information about rotation of the particle, as well as its transverse motion near the curved boundaries, responsible for any nontrivial effects, is comprised in the position-dependent effective diffusion coefficient $D(x)$ and the function $A(x)$. In the simplest case of a diffusing passive particle, it is interpreted as the Boltzmann factor of the entropic potential $U_e(x) = -\ln A(x)$. For active particles [36–38], additional terms appear in such potential. These terms reflect the stochastic self-propulsion and are directly related to the effective force driving the ratchet current. Hence, calculation of the ratchet current from the one-dimensional (1D) projected equation, Eq. (1.1), is much easier than solving the fully dimensional problem numerically.

The projection technique is based on scaling of the transverse coordinate(s) by a small parameter $\sqrt{\epsilon}$ (or equivalently, the diffusion coefficient by $1/\epsilon$). For the diffusion of a passive particles alone [42–44], the transverse relaxation in the limit $\epsilon \to 0$ becomes infinitely fast, immediately equilibrating (flattening) the transverse profile of the 2D probability density. Having integrated the 2D diffusion equation across the channel and applying the flattened profile, we arrive at the basic FJ equation (1.1) with $D(x) = D_T$ and $A(x) = 2h(x)$ [39]. The finite ϵ slows down the transverse relaxation, so the transverse profile starts to deflect from the equilibrium. These deviations of the 2D density, depending on $p(x,t)$, $h(x)$ and its derivatives, can be expressed as a series controlled by ϵ, calculated recursively. If applied in the integrated 2D diffusion equation, we obtain Eq. (1.1) with the spatial dependent $D(x)$ expanded in ϵ, including the corrections due to varying width of the channel and a nontrivial flow near the curved walls.

A similar procedure can be developed for our system with Janus particles. The corresponding Fokker-Planck equation is integrated not only across the channel, but also over the angle ϕ of the rotating disk. Thus ϕ has to be scaled, too, as well as the spatial transverse coordinate y (and the transverse force, [45,46]). The limit $\epsilon \to 0$, providing the infinitely fast transverse relaxation, makes also the rotation of the disk so fast that the self-propelling force acts in random direction, effectively with zero mean. The particle in this limit behaves as passive and thus the basic FJ approximation can be found. Nonzero $\epsilon > 0$, slowing rotation and transport to or from the boundaries, enables the self-propulsion to reflect the particle's hitting the walls, rectifying its motion. It is described by the corrections to the basic FJ. To derive them, one can adjust the mapping procedure formulated for confined diffusion driven by nonconservative forces [47]. It introduces a gauge function $\gamma(x)$ added to the entropic potential $U_e(x)$; its expansion in ϵ is derived recursively together with deviations from the zeroth order density and $D(x)$. For periodic profiles $h(x)$, the function $\gamma(x)$ can be decomposed in two contributions, the first being spatially periodic with the same period as $h(x)$, while the second is a linear function of x. It is the latter contribution that gives rise to the ratchet effect.

We formulate precisely the problem in Sec. II and develop the theory outlined above. In Sec. III, we arrive at analytic formulas for the effective force driving the ratchet effect, enabling us to determine easily the ratchet current. Then we test the results on a trial channel, asymmetric in the longitudinal direction; they are also verified by a numerical solution of the fully dimensional problem. By construction, our theory describes well the region of an asymptotically large ratio $\alpha = D_R/D_T$, i.e., the quickly rotating particles, exhibiting the decay of the current $J \sim 1/\alpha^2$. Validity of our formulas is also restricted to small driving forces f, taking only the leading terms $\sim f^2$. If we allow anisotropy of the driving force, the current reversal can be observed at some value of α.

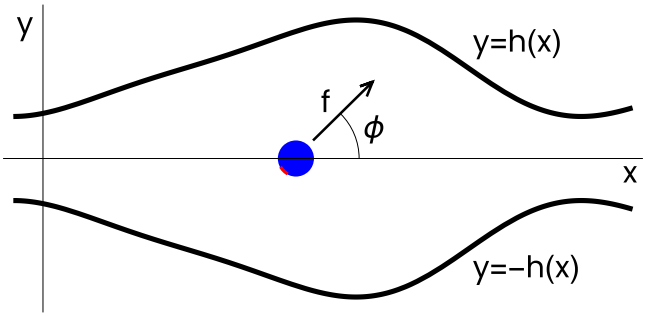

FIG. 1. Scheme of the considered device. An active (red) spot on the disk drives the particle in the opposite direction by the force f. The particle diffuses in a channel bounded by $-h(x) < y < h(x)$ and also rotates stochastically in the angle ϕ.

II. THE MAPPING PROCEDURE

We start with a definition of the model. The particle diffuses in a 2D channel symmetric with respect to the longitudinal x axis; its transverse position y is bounded by $-h(x) < y < h(x)$, see Fig. 1. The shaping function $h(x)$ is supposed analytic and positive. The particle is represented by a tiny disk of the radius negligible with respect to the typical half-width $h(x)$, rotating randomly in angle ϕ. The disk is self-propelled from some spot on its circumference by a force of constant magnitude F and the direction depending on the angle ϕ. So the fully dimensional probability density $\rho(x,y,\phi,t)$ depends on three spatial variables and time. It is governed by the Fokker-Planck equation

$$\partial_t \rho(x,y,\phi,t) = D_R \partial_\phi^2 \rho(x,y,\phi,t) + D_T[\partial_x(\partial_x - f\cos\phi) + \partial_y(\partial_y - f\sin\phi)]\rho(x,y,\phi,t), \tag{2.1}$$

describing the stochastic rotation of the disk and the translational diffusion driven by the force $f = F/k_BT$ acting in the angle ϕ; T is the temperature. The rotation and the translation parts are proportional to the diffusion constants D_R and D_T, respectively. The time can be rescaled by the diffusion constant, $D_T t \to t$, then D_R is replaced by the ratio $\alpha = D_R/D_T$. Equation (2.1) is supplemented by the no-flux boundary conditions (BC)

$$[(\partial_y - f\sin\phi) \mp h'(x)(\partial_x - f\cos\phi)]\rho(x,y,\phi,t)|_{y=\pm h(x)} = 0 \tag{2.2}$$

at both boundaries for any angle ϕ; we also require periodicity $\rho(x,y,\phi,t) = \rho(x,y,\phi+2\pi,t)$.

The key point of the mapping is the controlling of the transverse diffusion by a small dimensionless parameter ϵ. In the case of the translation diffusion alone [42–44], typically the transverse lengths y, $h(x)$ are scaled as $y \to \sqrt{\epsilon}y$, making the transverse relaxation infinitely fast in the limit $\epsilon \to 0$. Consistently for the driven diffusion, the transverse component of the force, has to be scaled inversely, $f \sin\phi \to (f \sin\phi)/\sqrt{\epsilon}$, keeping the scalar potential $U_\phi(x, y) = -f(x \cos\phi + y \sin\phi)$ unscaled [45,46] for a given ϕ. For the Janus particles, Eq. (2.1), we intend to consider the angle ϕ as the next transverse coordinate, but its scaling looks dubious. Still, we can apply an alternative interpretation: scaling of the transverse lengths by $\sqrt{\epsilon}$ is equivalent to introducing anisotropy of the diffusion constant D_T by scaling its transverse component to D_T/ϵ. Correspondingly, we have to introduce also an auxiliary anisotropy of the force $\vec{f} = (f \cos\phi, g \sin\phi)$, where the transverse amplitude $g = \sqrt{\epsilon}f$ corresponds to the (scaled) isotropic case. Now we can consider the angle ϕ as another "transverse" coordinate by scaling $D_R \to D_R/\epsilon$, or equivalently, we define the scaled ratio $q^2 = \epsilon\alpha = \epsilon D_R/D_T$ in Eq. (2.1). Finally, we arrive at the scaled equation

$$\partial_t \rho = \left[\partial_x(\partial_x - f\cos\phi) + \frac{1}{\epsilon}\partial_y(\partial_y - g\sin\phi)\right]\rho + \frac{q^2}{\epsilon}\partial_\phi^2\rho, \tag{2.3}$$

supplemented by the BC

$$[(\partial_y - g\sin\phi) \mp \epsilon h'(x)(\partial_x - f\cos\phi)]\rho|_{y=\pm h(x)} = 0; \tag{2.4}$$

the prime denotes the derivative according to x.

Our aim is to reduce Eqs. (2.3), (2.4) to an equation in the only spatial coordinate x, governing the marginal (1D) density

$$p(x,t) = \int_0^{2\pi} d\phi \int_{-h(x)}^{h(x)} \rho(x, y, \phi, t)dy. \tag{2.5}$$

Integrating Eq. (2.3) over y and ϕ, using integration by parts, periodicity of ρ in ϕ and BC (2.4), we get

$$\partial_t p(x,t) = \partial_x\left[\partial_x p(x,t) - \int_0^{2\pi} d\phi\left(h'(x) \times [\rho(x, h(x), \phi, t) + \rho(x, -h(x), \phi, t)] + f\cos\phi \int_{-h(x)}^{h(x)} \rho(x, y, \phi, t)dy\right)\right]. \tag{2.6}$$

The crucial task now is to express $\rho(x, y, \phi, t)$ using $p(x, t)$ to close the equation.

The first step is the basic FJ approximation. In the limit $\epsilon \to 0$, the relaxation across the channel as well as the stochastic rotation of the disk becomes infinitely fast. Still, finding the corresponding zeroth order density $\rho_0(x, y, \phi, t)$ is not trivial. The equilibrium for a given orientation ϕ is proportional to $\exp[-U_\phi(x, y)]$, but also ϕ is changing rapidly, influencing the density ρ_0 depending on the ratio q^2 between the fast rotation and translation diffusions. The searched ρ_0 can be found by solving Eq. (2.3) with BC (2.4) in the limit $\epsilon \to 0$, i.e., keeping only the terms $\sim 1/\epsilon$,

$$\left[q^2\partial_\phi^2 + \partial_y(\partial_y - g\sin\phi)\right]\rho_0 = 0, \quad (\partial_y - g\sin\phi)\rho_0|_{y=\pm h(x)} = 0. \tag{2.7}$$

The solution periodic in ϕ can be found in the form of expansion in powers of g, namely,

$$\rho_0 = \left[1 + g\frac{\sinh qy \sin\phi}{q\cosh qh} + g^2\left(\frac{qh\cosh qy - \sinh qh}{2q^3 h\cosh qh} + \frac{(\cosh qh\cosh qy - \cosh 2qy)\cos 2\phi}{6q^2\cosh^2 qh}\right) + \cdots\right] \times \frac{p(x,t)}{A_0(x)} = \omega_0(x, y, \phi)\frac{p(x,t)}{A_0(x)}, \tag{2.8}$$

see the Appendix for more details. For brevity, we omit writing the obvious arguments; the dots "$\cdots$" denote here the higher order terms in g. The factor $p(x, t)/A_0(x)$ is an integration constant (in the variables y and ϕ); it is fixed to make the normalization (2.5) consistent, hence

$$A_0(x) = 4\pi h(x). \tag{2.9}$$

Applying the (pseudo-)equilibrated density ρ_0, Eq. (2.8), in the integrated equation (2.6), we obtain the basic FJ equation after some algebra,

$$\partial_t p = \partial_x\left[A_0\partial_x - 4\pi h'\left(g^2\frac{(qh - \tanh qh)}{2q^3 h} - \cdots\right)\right]\frac{p}{A_0}. \tag{2.10}$$

Unlike the mapping of the diffusion alone [42,43] or in a conservative field [45,46], the use of A_0 fixed by normalization does not convert here the mapped equation to the FJ form (1.1). Similar to diffusion driven by the vortex forces [47], one has to calibrate $A_0(x)$ by some function $\gamma_0(x)$, $A_{FJ}(x) = A_0(x)e^{\gamma_0(x)}$, to eliminate the terms not containing the derivative ∂_x in the square brackets of Eq. (2.10). Then after setting

$$\gamma_0'(x) = \frac{h'}{h}\left(g^2\frac{(qh - \tanh qh)}{2q^3 h} - \cdots\right), \tag{2.11}$$

we transform Eq. (2.10) into the desired form $\partial_t p = \partial_x A_{FJ}\partial_x(p/A_{FJ})$.

For $\epsilon > 0$, the transverse diffusion and rotation of the disk become slower, unable to relax the full dimensional density $\rho(x, y, \phi, t)$ to ρ_0 immediately after any changes of $p(x, t)$. We express formally the deviations from ρ_0 by a series of corrections controlled by ϵ,

$$\rho(x, y, \phi, t) = e^{\gamma(x)}\hat{\omega}\frac{p(x,t)}{A(x)} = e^{\gamma(x)}\sum_{n=0}^{\infty}\epsilon^n\hat{\omega}_n\frac{p(x,t)}{A(x)}; \tag{2.12}$$

each of them calculated by an operator $\hat{\omega}_n(x, y, \phi, \partial_x)$ acting on the solution $p(x, t)/A(x)$ of the reduced 1D problem. Again, we introduced here $A(x)$ instead of $A_0(x)$, which is now calibrated by a function $\gamma(x)$ also expanded in ϵ,

$$A(x) = A_0(x)e^{\gamma(x)} = A_0(x)\exp\left[\sum_{n=0}^{\infty}\epsilon^n\gamma_n(x)\right], \tag{2.13}$$

enabling us to write the final mapped equation in the desired FJ form. We find below that except for the zeroth order $\hat{\omega}_0 = \omega_0$, Eq. (2.8), the higher correcting operators $\hat{\omega}_n$ also contain the derivatives ∂_x^k up to the $k = n$-th order. It is convenient to separate the term which does not contain

the derivatives, splitting the expression as $\hat{\omega}_n(x, y, \phi, \partial_x) = \tilde{\omega}_n(x, y, \phi, \partial_x)\partial_x + \omega_n(x, y, \phi)$, where the last term is just a bare function.

Applying the relations above in Eq. (2.6), we get

$$\partial_t p(x,t) = \partial_x A(x)\Bigg[\partial_x + \frac{A_0'(x)}{A_0(x)} + \gamma'(x) - \int_0^{2\pi}\frac{d\phi}{A_0(x)} \times \Bigg(h'(x)[\hat{\omega}(x, h(x), \phi, \partial_x) + \hat{\omega}(x, -h(x), \phi, \partial_x)] + f\cos\phi\int_{-h(x)}^{h(x)} dy\, \hat{\omega}(x, y, \phi, \partial_x)\Bigg)\Bigg]\frac{p(x,t)}{A(x)}. \tag{2.14}$$

The form of the generalized FJ equation [45–47],

$$\partial_t p(x,t) = \partial_x A(x)[1 - \hat{Z}(x, \partial_x)]\frac{p(x,t)}{A(x)},$$
$$\hat{Z}(x, \partial_x) = \sum_{n=1}^{\infty}\epsilon^n \hat{Z}_n(x, \partial_x), \tag{2.15}$$

is achieved after eliminating the functional parts $\omega_n(x, y, \phi)$ by the proper choice of $\gamma_n'(x)$ in each order of ϵ^n; the remaining terms containing $\tilde{\omega}_n$ define $\hat{Z}_n$. In the zeroth order we recover Eq. (2.11), while in the higher orders we have

$$\gamma_n'(x) = \int_0^{2\pi}\frac{d\phi}{A_0(x)}\Bigg[h'(x)\Big(\omega_n|_{y=h(x)} + \omega_n|_{y=-h(x)} + f\cos\phi\int_{-h(x)}^{h(x)}\omega(x, y, \phi)dy\Big)\Bigg],$$
$$\hat{Z}_n(x, \partial_x) = \int_0^{2\pi}\frac{d\phi}{A_0(x)}\Bigg[h'(x)\Big(\tilde{\omega}_n|_{y=h(x)} + \tilde{\omega}_n|_{y=-h(x)} + f\cos\phi\int_{-h(x)}^{h(x)}\tilde{\omega}(x, y, \phi, \partial_x)dy\Big)\Bigg]. \tag{2.16}$$

Finally, the operators $\hat{\omega}_n$ are calculated within the recurrence procedure based on a requirement that the density $\rho(x, y, \phi, t)$, obtained from any 1D solution $p(x, t)$ of Eq. (2.15) by the backward mapping relation (2.12), has to satisfy the original fully dimensional problem, Eqs. (2.3), (2.4). Substituting there accordingly and expressing the terms $\sim 1/\epsilon$, we find

$$\frac{1}{\epsilon}\big[\partial_y(\partial_y - g\sin\phi) + q^2\partial_\phi^2\big]\hat{\omega}\frac{p}{A} = \Bigg[\hat{\omega}\frac{1}{A}\partial_x A(1 - \hat{Z})\partial_x - e^{-\gamma}\partial_x(\partial_x - f\cos\phi)e^{\gamma}\hat{\omega}\Bigg]\frac{p}{A}. \tag{2.17}$$

The time derivative ∂_t is commuted here with the spatial operators to the right up to $\partial_t p$, which is replaced by the right-hand side (RHS) of Eq. (2.15). This equation has to be satisfied for any p/A, so it relates the operators $\hat{\omega}_n$. Expanding $\hat{\omega}$, γ, and $\hat{Z}$ in ϵ and collecting the terms at the same powers ϵ^n, we obtain the recurrence relations for $\hat{\omega}_{n+1}$.

Let us demonstrate the calculation on the first order. The terms $\sim\epsilon^0$ give the operator equation for $\hat{\omega}_1$,

$$\big[\partial_y(\partial_y - g\sin\phi) + q^2\partial_\phi^2\big]\hat{\omega}_1 = \omega_0\Bigg[\partial_x + \frac{A_0'}{A_0} + \gamma_0'\Bigg] - e^{-\gamma_0}\partial_x(\partial_x - f\cos\phi)e^{\gamma_0}\omega_0 = R_{1,1}(x, y, \phi)\partial_x + R_{1,0}(x, y, \phi); \tag{2.18}$$

commutation of ∂_x on the RHS to the right and applying Eqs. (2.8)–(2.11) for ω_0, A_0 and γ_0' result in the explicit formulas for the functions $R_{1,1}$, $R_{1,0}$. Then the partial differential equation is solved by $\hat{\omega}_1$ expanded in g, also satisfying the BC (2.4) taking the terms $\sim\epsilon^1$, see the Appendix for details. The formulas for $\hat{\omega}_1$ are rather complicated even in the lowest orders of g; the leading terms $\sim g^0$ are

$$\hat{\omega}_1 = \Bigg[(3y^2 - h^2)\frac{h'}{6h} - \frac{f\cos\phi}{q^2} + \cdots\Bigg]\partial_x - \frac{fh'\cosh qy\cos\phi}{q\sinh qh} + \cdots. \tag{2.19}$$

The result has the expected structure $\hat{\omega}_1 = \tilde{\omega}_1\partial_x + \omega_1$, so we can apply the formulas (2.16) to obtain

$$\hat{Z}_1 = \frac{h'^2}{3} - \frac{f^2}{2q^2} - \frac{g^2h'^2}{12q^5h^3}\Bigg[3\tanh qh - 3qh(1 + \tanh^2 qh) + 6q^2h^2\frac{\tanh qh}{\cosh^2 qh} - 2q^3h^3\Big(\frac{2}{\cosh^2 qh} - 1\Big)\Bigg] + \cdots, \tag{2.20}$$

$$\gamma_1' = -\frac{f^2h'}{2q^2h} + \frac{g^2h'}{12q^5h^2}\Bigg[qh''\tanh qh\Big([3 - 2q^2h^2]\tanh qh - \frac{3qh}{\cosh^2 qh}\Big) + q^2h'^2\Big(3\tanh qh - \frac{qh}{2\cosh^4 qh}[\cosh 4qh - 3\cosh 2qh + 8 + 4qh\sinh 2qh] + 3f^2(\tanh qh - qh)\Big)\Bigg] + \cdots, \tag{2.21}$$

up to the order $\sim g^2$. Complexity of the formulas quickly grows with growing orders in g, as well as ϵ, so we restrict our calculations to the terms $\sim f^2$ and $\sim g^2$, i.e., the results are valid for small self-propelling forces. For our next considerations, we need yet the term $\sim g^0\epsilon^2$,

$$\gamma_2' = \frac{f^2}{12q^4h^2}[2qh'^3(2qh - 3\coth qh) + 2h'h''(q^2h^2 + 3qh\coth qh + 3) - 6hh^{(3)} + 3f^2hh'] + \cdots. \tag{2.22}$$

Notice that integration of the derivatives $\gamma_n'(x)$ is not necessary within the recurrence procedure.

It is worth to analyze some important limits of the rather complicated formulas (2.20)–(2.22). The term $h'^2/3$ in $\hat{Z}_1$, independent of the driving force, reproduces the leading Zwanzig-Reguera-Rubí (ZRR) correction to the diffusion coefficient $D(x)$ in corrugated channels for the diffusion alone [40,41]. The second term $-\epsilon f^2/2q^2 = -f^2/2\alpha$ corresponds to the leading correction of $D(x)$ due to the flipping longitudinal force [37] (notice that α means there the frequency of the flipping, which is analogous but not identical to $\alpha = D_R/D_T$ here).

Let us recall that after the scaling of $\alpha = q^2/\epsilon$, the expansion of $\hat{Z}$ and γ in ϵ means correcting their values for infinitely fast stochastic rotation due to (small) nonzero $1/\alpha$. So our results describe well especially the region of large α and it is useful to look for their asymptotics in the limit $\alpha \to \infty$. For $\hat{Z}_1$, we get

$$\epsilon\hat{Z}_1 \simeq \frac{\epsilon}{3}h'^2 - \frac{f^2}{2\alpha} - \frac{g^2}{6\alpha}h'^2 + \cdots . \tag{2.23}$$

As we are also restricted to consider only a small transverse force g because of truncation of our series above g^2, the corrections of $\hat{Z}$ due to the self-propelling force become negligible with respect to the ZRR terms [41,43],

$$1/D_{ZRR}(x) = (1+\epsilon h'^3)^{1/3} \simeq 1 + \epsilon h'^2/3 + \cdots , \tag{2.24}$$

which will be used in our next calculations.

We focus our analysis mainly on the function $\gamma(x)$. Equation (1.1) can be interpreted as the Smoluchowski equation with a varying diffusion coefficient $D(x)$, then $-\gamma(x)$ becomes a part of the 1D effective potential. Its derivative represents the local force effectively driving the particle along the channel, also giving rise to the ratchet current. Notice that $\gamma_n' = 0$ for zero f, g. Keeping the unscaled $\alpha = q^2/\epsilon$ finite and $g = \sqrt{\epsilon} f$, we obtain the terms

$$\epsilon\gamma_1' + \epsilon^2\gamma_2' \to -\left(\frac{f^2}{2\alpha} - \frac{f^4}{4\alpha^2}\right)\frac{h'}{h} - \frac{f^2}{2\alpha^2}\left(\frac{h'^3}{h^3} - \frac{2h'h''}{h^2} + \frac{h^{(3)}}{h}\right)$$

in the spatial FJ limit, $\epsilon \to 0$, corresponding to the comparable terms of γ in the model of fluctuating longitudinal force [36,37]. It is useful again to find the asymptotics of γ_n' for large α at a fixed nonzero ϵ,

$$\begin{aligned}\gamma_1' &= -\frac{f^2 h'}{2q^2 h} - \frac{g^2}{q^2}\left(\frac{h'^3}{3h} + \frac{h'h''}{6} - \frac{h'^3}{4qh^2} - \frac{h'h''}{4q^2h^2}\right) + \cdots ,\\ \gamma_2' &= \frac{f^2}{q^2}\left(\frac{h'^3}{3h} + \frac{h'h''}{6} - \frac{h'^3}{2qh^2} + \frac{h'h''}{2qh} + \frac{h'h''}{2q^2h^2} - \frac{h^{(3)}}{2q^2h}\right)\\ &\quad + \cdots ,\end{aligned} \tag{2.25}$$

$q^2 = \epsilon\alpha$. Notice that for the scaled isotropic force, $g = \sqrt{\epsilon} f$, the terms $\sim\epsilon^k g^0$, $\epsilon^{k-1}g^2$, …, $\epsilon^0 g^{2k}$ sum with one another; all of them have to be derived to receive a consistent result. Specifically here, the terms $\sim g^2/q^2$ and f^2/q^2 in γ_1' and γ_2', respectively, cancel one another, influencing finally the power-law asymptotics.

Finally, let us comment dimensionality of the problem. Rescaling the time by D_T and the force by k_BT, we are working with only lengths here; the dimension of f, q, $\sqrt{\alpha}$ is the inverse length. The length unit is left arbitrary; it is convenient to derive it from the period of the channel ($L = 1$ or 2π). Then f reflects the energy of a particle gained by driving over L and α says about the mean squared angle in which the particle rotates while the spatial mean squared displacement reaches L^2. The formulas for $\hat{Z}_n$ and γ_n' point to other important quantities, f/q influencing the convergence of the expansion, or the mean $h(x)q$, restricting validity of the asymptotic behavior. Still, usability of our (truncated) expansion is also determined by the shape of the channel, i.e., the derivatives of $h(x)$, similar to the mapped spatial diffusion alone [48,49].

III. THE RATCHET EFFECT

We demonstrate now the appearance of the ratchet effect in a periodic corrugated channel shaped by the function $h(x) = h(x+L)$, where L is the spatial period. The ratchet current is driven by the nonzero increment of the effective 1D potential $U_e(x) = -\ln A_0(x) - \gamma(x)$. Because $A_0(x)$ is always periodic with the same period as $h(x)$, the non-zero increment originates solely from the gauge function $\gamma(x)$. For the mirror-asymmetric shape $h(x)$ we can get a nonzero increment $\Delta\gamma = \gamma(x+L) - \gamma(x)$ over one period L, which determines the effective 1D mean force driving the ratchet current. It reflects the hits of the particles to the walls, rectifying the self-propulsion $\vec{f}$ (whose value averaged over the orientation ϕ is zero).

The increasing components of γ appear after an integration of $\gamma_n'(x)$, derived by the mapping procedure. It is easy to see that $\gamma_0(x)$ has no such component. Its derivative (2.11) is of the form $\gamma_0'(x) = G_0[h(x)]h'(x)$, hence $\gamma_0(x) = \int G_0[h(x)]h'(x)dx = \int G_0[h]dh$ is explicitly a function of only $h(x)$ and so periodic. In the higher orders, we analyze the asymptotics (2.25) for the isotropic force, $g = \sqrt{\epsilon} f$. Integrating the leading contributions to $\gamma(x)$, Eqs. (2.25):

$$\begin{aligned}\epsilon\gamma_1 + \epsilon^2\gamma_2 + \cdots &= \int\left[-\frac{\epsilon f^2 h'}{2qh} + \frac{\epsilon^2 f^2}{2q^3}\left(\frac{h'h''}{h} - \frac{h'^3}{2h^2}\right.\right.\\ &\quad \left.\left. + \frac{3h'h''}{2qh^2} - \frac{h^{(3)}}{qh}\right) + \cdots\right]dx\\ &= -\frac{\epsilon f^2}{2q^2}\ln h + \frac{\epsilon^2 f^2}{2q^4}\left(\frac{qh'^2}{2h} - \frac{h''}{h}\right.\\ &\quad \left. + \frac{h'^2}{4h^2} + \int\frac{h'^3}{2h^3}dx\right) + \cdots ,\end{aligned} \tag{3.1}$$

we find a term, which cannot be expressed explicitly for a generic $h(x)$. Unlike the other terms composed from the derivatives of $h(x)$ and so periodic, it can give the nonzero increment

$$\Delta\gamma = \frac{f^2}{4\alpha^2}\int_0^L \frac{h'^3}{h^3}dx + \cdots \tag{3.2}$$

in the channels with asymmetric $h(x)$; it is demonstrated on a trial function below. Notice that for symmetric channels, $h(x) = h(L-x)$, this integral [and similar in the higher orders, e.g., Eq. (A6)] are zero; the ratchet effect is caused by breaking the mirror symmetry $x \leftrightarrow -x$ of the channel [50,51].

Thus in 1D projection, we observe diffusion in a slanted washboard potential $U_e(x) = -\ln A_0(x) - \gamma(x)$ modified by the position-dependent diffusion coefficient $D(x)$. Assuming normalization by one particle per period L, the stationary current can be expressed using the Stratonovich [52,53] or the Lifson-Jackson [54] formulas

$$\begin{aligned}J &= (1-e^{-\Delta\gamma})\left[\int_0^L A(x)dx\int_x^{L+x}\frac{dx'}{A(x')D(x')}\right]^{-1}\\ &\simeq \Delta\gamma\left[\int_0^L A_0(x)e^{\gamma(x)}dx\int_0^L\frac{e^{-\gamma(x)}dx}{A_0(x)D(x)}\right]^{-1},\end{aligned} \tag{3.3}$$

(the last one holds for small $\Delta\gamma$); see the Appendix.

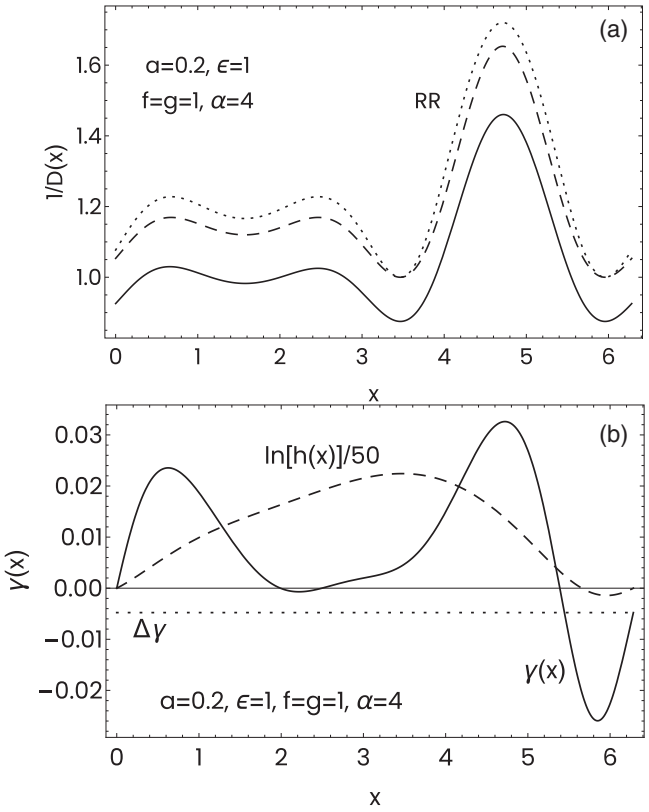

FIG. 2. (a) Inverse effective diffusion coefficient $1/D(x)$ according to Eq. (2.20) (solid line) for the trial shaping function (3.4), compared to the Reguera-Rubí formula (2.24) (dotted line) and its first order (Zwanzig) approximation (dashed line). (b) Correction $\gamma(x)$ (solid line) to the entropic potential $\sim \ln h(x)$ (dashed line), obtained by integration of Eqs. (2.11), (2.21), and (2.22) for the same function and parameters. The dotted line marks decrement of $\gamma(x)$ over one period.

Our theory is demonstrated on the shaping function

$$h(x) = 2 - \cos x + a \sin 2x, \tag{3.4}$$

depicted in Fig. 1. Asymmetry of the channel is controlled by the parameter a; we used $a = 0.2$. Figures 2(a) and 2(b) show the functions $1/D(x)$ and $\gamma(x)$, respectively, which enter the generalized FJ equation (1.1). The effective diffusion coefficient $D(x)$ [Fig. 2(a)] is calculated here for a large force $f = g = 1$ and rather small $\alpha = 4$ in order to better visualize the effect of the self-propelling force. Its main effect is the shift of the function $1/D(x)$ by an amount proportional to f^2/α [see Eq. (2.23)], with respect to $1/D(x)$ valid for the diffusing passive particle, which is well approximated by the Reguera-Rubí formula (dotted line). For $f = 0.1$ and large α, as considered in our next calculations, this shift becomes negligible and we use Eq. (2.24). Figure 2(b) depicts the function $\gamma(x)$ (solid line) integrated up to the second order, Eq. (2.22), for the same parameters ($f = g = 1$ and $\alpha = 4$), compared with $\ln h(x)$ proportional to the entropic potential. We can observe a tiny decrement $\Delta\gamma \simeq -0.00478$ over one period, which effectively drives the ratchet current.

Figure 3 describes the decrement $|\Delta\gamma|$ (divided by f^2 to enhance the leading terms, the left scale) depending on the

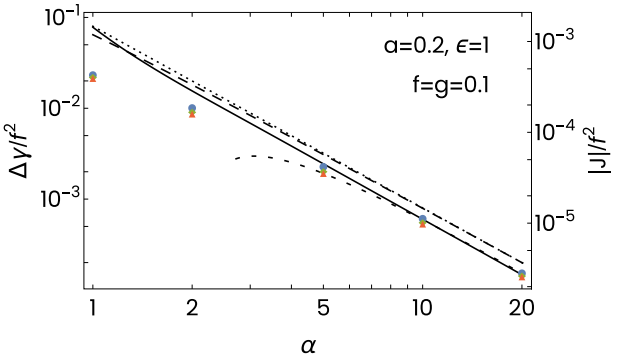

FIG. 3. Potential decrement $\Delta\gamma$ over one period of the channel (3.4) (the left scale) and the corresponding ratchet current J, Eq. (3.3) for one particle per period (the right scale), depending on the ratio $\alpha = D_R/D_T$ of the rotation and translation diffusion constants of the Janus particle. The long dashed line describes the results up to the second order according to Eqs. (2.21) and (2.22); the next order is added in the solid line. The dotted and the short dashed lines correspond to the asymptotics (3.2) and with Eq. (A6) added, respectively. The numerical solutions of the fully dimensional problem are depicted by the orange triangles ($f = 0.1, 0.2, 0.5$), green diamonds ($f = 1$), and blue disks ($f = 2$).

ratio $\alpha = D_R/D_T$, calculated by various methods. The right scale assigns the corresponding values of the ratchet current J of all depicted lines using the Lifson-Jackson formula (3.3) with $1/D(x)$ approximated by Eq. (2.24), making the mobility $\sim J/\Delta\gamma$ almost constant, depending only on geometry of the channel. The calculated lines are compared with numerical solutions of the fully dimensional problem (2.1) (color marks). The numerical data are almost identical in a wide range of the force f, from 0.1 (red triangles) to 2 (blue disks), what indicates that the leading terms $\sim f^2$ or g^2 are dominant and truncating our series in g^2 is justified. The leading contribution to $\Delta\gamma$ (or the current J, long dashed line) obtained by numerical integration of Eqs. (2.21), (2.22) is very well approximated by the asymptotics (3.2) (dotted line), but both give slightly shifted results with respect to the numerical data. This difference is satisfactorily corrected by the next terms $\sim\epsilon^2 g^2$ and $\epsilon^3 g^0$ (full line), which are already too complicated; their asymptotics (short-dashed line), added to the formula (3.2) are stated in the Appendix. As expected, Fig. 3 documents that our theory describes well especially the region of large α, i.e., particles whose angular diffusion is much faster than the spatial diffusion. We can see that for the parameters of the channel we use, our predictions hold well till $\alpha > 4$. The range of usability of our formulas does, of course, depend on the specific shape of the channel given by the function $h(x)$.

Figure 4 shows the usability of the results depending on the scaling parameter ϵ; the self-propelling force is kept isotropic, $g = \sqrt{\epsilon} f$. A smaller ϵ improves convergence of the series, and so also the dominance of the considered leading terms. On the other hand, $\epsilon \to 0$, also included in $q = \sqrt{\epsilon\alpha}$ in the formulas for $\gamma_n'(x)$, has the same effect as taking α small, i.e., out of the region where the expansion is applicable. Similar to the ratchets driven by the fluctuating dichotomic force [37], we see optimum reliability for ϵ slightly smaller than 1 for the presented geometry.

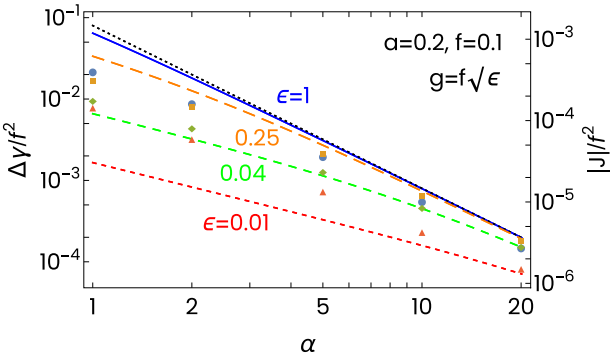

FIG. 4. Potential decrement $\Delta\gamma$ over one period and the ratchet current J vs. $\alpha = D_R/D_T$ for $\epsilon = 1$ (blue), 0.25 (orange), 0.04 (green), and 0.01 (red), calculated according to Eqs. (2.21) and (2.22) (dashed and solid lines). The asymptotics (3.2) is described by the dotted line. The symbols (red triangles, green diamonds, orange squares, and blue disks) depict the numerical data for the corresponding values of ϵ.

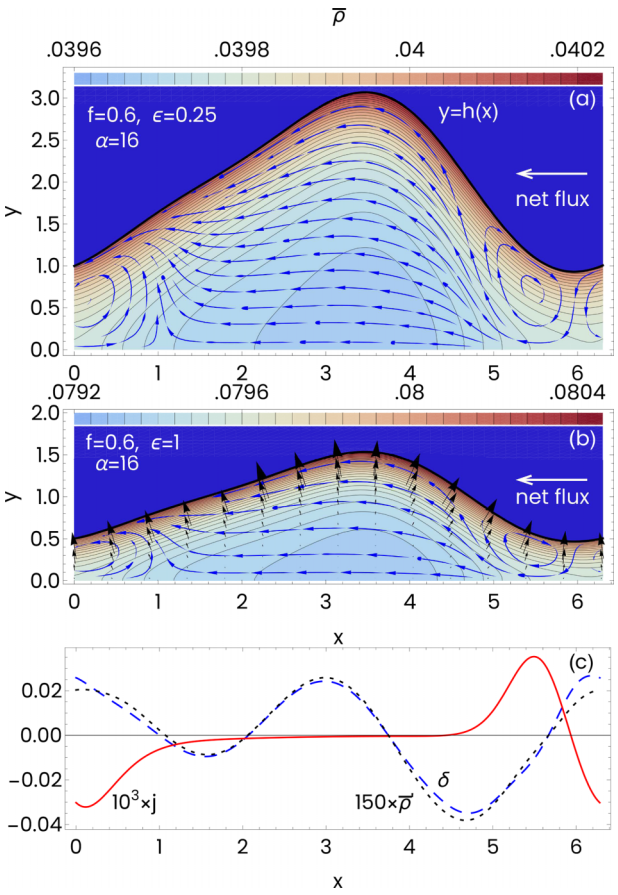

FIG. 5. (a) Contour plot of the 2D density $\bar{\rho}(x, y)$ averaged over the orientation of the force (color scale) in the upper half-channel shaped by $h(x)$, Eq. (3.4), $\epsilon = 0.25$ and $g = f/2$. The streamlines depict the corresponding averaged current density $\vec{j}(x, y)$. (b) The same plot for the channel shaped by $h(x)/2$, but with $\epsilon = 1$ and $g = f$. Black arrows here depict polarization. The net flux in both cases $J = -6.33 \times 10^{-6} f^2$ (c) Deflection δ of the polarization from the normal to the boundary (in radians, dashed line), gradient of the averaged density along the boundary, $\bar{\rho}' = d\bar{\rho}[x, h(x)]/dx$ (dotted line), and the current density j at the boundary (solid line).

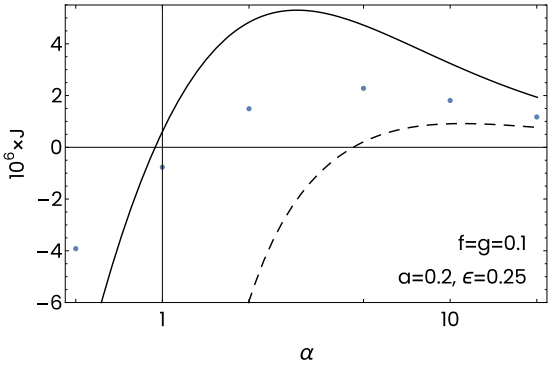

FIG. 6. The ratchet current J vs. α for an anisotropic self-propulsion; $g = 0.1 > \sqrt{\epsilon} f = 0.05$. Full line represents the leading terms, given by Eqs. (2.21), (2.22), the dashed line contains the next order corrections added. The dots depict the numerical solution of the problem.

The 2D density $\bar{\rho}(x, y)$ averaged over the orientation ϕ of the force f, as well as the averaged flux densities, are shown in Fig. 5(a) (color scale and streamlines, respectively). They are calculated within the backward mapping, Eq. (2.12), (see the Appendix for details) for $\epsilon = 0.25$ and isotropic scaling, $g = f/2 = 0.3$. The expected accumulation of the particles near the boundaries is observed, especially at the extremities of the width of the channel, which act effectively as traps. Although it cannot be easily seen by a qualitative analysis, the active particles can escape from these traps more easily in one direction than in the opposite one. This behavior depends on the asymmetry of the function $h(x)$ and gives rise to the ratchet current. Figure 5(b) shows the same plot for the channel twice narrower (shaped by the function $h(x)/2$), but isotropic, $\epsilon = 1$ and $g = f$. The same net flux J, distribution of the density $\bar{\rho}$, as well as the flux patterns are observed. It demonstrates physical meaning of the scaling; taking $\epsilon < 1$ describes an isotropic channel $\sqrt{\epsilon}$-times narrower with the transverse component of the force scaled as $g = \sqrt{\epsilon} f$.

We also looked at the local polarization $\vec{P}(x, y) = \int \vec{f}(\phi)\rho(x, y, \phi)d\phi / \int \rho(x, y, \phi)dxdyd\phi$ (see the Appendix for details of the computation) which is depicted by black arrows in Fig. 5(b). We can see that the absolute value of the polarization increases from the center toward the walls. Just at the walls, it is nearly, but not exactly, perpendicular to the walls. In Fig. 5(c) we show (dashed line) the tiny deflections δ from the normal direction depending on the curvature of the shaping $h(x)$. The deflection δ strongly correlates with the gradient of the density along the boundary, measured by the derivative $d\bar{\rho}[x, h(x)]/dx$ (dotted line in Fig. 5(c)). The resulting flux along the boundary appears due to a subtle imbalance of the internal driving (measured by polarization) and the gradient of the density.

Finally, we touch on the possibility of the current reversal in this model. This question arose in the study of the particles driven by the fluctuating dichotomic transverse force in a corrugated 2D channel [38]. The corresponding ratchet current flows in the opposite direction in comparison to the longitudinal driving in the same geometry [37]. The results presented for the isotropic force with the transverse compo-

nent scaled as $g = \sqrt{\epsilon} f$ exhibit monotonic decay $\sim\alpha^{-2}$ for large $\alpha = D_R/D_T$. To test the possible appearance of current reversal, we artificially introduce the anisotropy in the driving force, setting $g > \sqrt{\epsilon} f$. As we see in Fig. 6, the transverse component pushing the particles to the right for larger α is overcome by influence of the longitudinal component, inverting direction of the current in smaller α. However, the supposed anisotropy of the force strongly harms convergence (and reliability) of our truncated series, but still, the effect of the current reversal, also supported by the numerical solution of the fully dimensional problem (dots), remains visible.

IV. CONCLUSION

We presented here a study of dynamics of active Janus particles moving in a 2D channel bounded by functions $-h(x) < y < h(x)$ varying in the longitudinal coordinate x. We focused especially on the appearance of the ratchet effect in periodic but mirror-asymmetric $h(x)$. We showed that the motion of the active particles can be mapped on a strictly 1D problem of a passive Brownian particle in an effective potential $-\ln A(x)$ and with position-dependent diffusion coefficient $D(x)$.

Our mapping method extends the technique of dimensional reduction developed for simpler systems, as passive particles diffusing alone [42,43], driven by conservative [45,46] or vortex forces [47]. The technique projects out the transverse coordinates, deriving the 1D generalized FJ equation (1.1). Its coefficients $A(x)$ and $D(x)$ involve information about the transverse motion of particles, causing peculiarities of the transport along the channel. They are calculated recursively, expanded in a small parameter ϵ, scaling the diffusion constants in the transverse directions. We showed here that the angular coordinate, describing direction of the self-propelling force of the Janus particle, can be considered as an additional transverse coordinate and treated on the same basis as the spatial transverse diffusion.

Although ϵ can be understood just as an auxiliary parameter, controlling the recurrence procedure, it is worth also to discuss its possible physical interpretation. Basically, it represents the ratio between the longitudinal and transverse diffusion constant, which is equivalent to a scaling of the transverse lengths (and correspondingly the forces) by $\sqrt{\epsilon}$, as shown in Figs. 5(a) and 5(b). So it is often interpreted as the ratio between the typical transverse and longitudinal lengths. Then the parameter $\alpha = D_R/D_T$, the ratio between the rotational and translational diffusion constants, can be compared to the number of orbits the particle makes while diffusing along the typical longitudinal length, e.g., the period of the channel. Finally, introducing $q^2 = \epsilon\alpha$, representing the scaling of the angular diffusion constant, enables us to collect the relevant correction terms with the same power of ϵ in the final formulas for $A(x)$ and $D(x)$. On the other hand, let us note that for a fixed finite q, taking a small value of ϵ simultaneously restricts the validity of the expansion to large α.

The mapping procedure generates an effective 1D potential $-\ln A(x) = -\ln A_0(x) - \gamma(x)$. Unlike the passive particle diffusing in a conservative field, the standard entropic contribution $-\ln A_0(x)$ is extended here by the gauge term $\gamma(x)$ in an analog to the system of particles driven by a nonconservative force [47]. We found that $\gamma(x)$ expanded in ϵ has the form of a slanted washboard potential; its increment $\Delta\gamma$ over one spatial period drives the nonzero ratchet current. Then the net flux is calculated straightforwardly using the Stratonovich or the Lifson-Jackson formulas (3.3). So the ratchet current can be estimated within our theory from a simple formula (3.2), which is its main advantage in comparison to questionable qualitative analyses or lengthy numerical computations. We compared our results up to the order $\sim\epsilon^3 f^2$ with the direct numerical solution of the original 2D problem of the Janus particle; a very good agreement is observed for larger parameters $\alpha > 4$ in our trial geometry (3.4). The leading nonzero term of $\Delta\gamma$ of order ϵ^2 determines the asymptotics of the ratchet current $J \sim 1/\alpha^2$ for $\alpha \to \infty$, which is also verified numerically.

The backward mapping onto the 2D problem enables us to obtain the full distribution of particles in the channel, Fig. 5. We observed the expected accumulation of particles at the walls and their minimum density at the axis of the channel. The complex vortices of the particle current density appear due to the interplay of active propulsion and the concentration gradient in a confined geometry.

Our method is by construction suitable for large values of the parameter α, i.e., for rapidly rotating particles. In practice, however, α is determined by the physical properties of the system, like the size of the particles, viscosity of the surrounding liquid. So, it would be desirable to continue the calculation somehow to the range of smaller α. In principle, this may be achieved by finding directly a differential equation for $\gamma(x)$, avoiding the expansion in ϵ, as suggested in the Appendix of Ref. [36] for a simpler ratchet model driven by the fluctuating longitudinal force only. It can serve as an inspiration for our study in the future.

ACKNOWLEDGMENTS

Support from VEGA Grant No. 2/0044/21 is gratefully acknowledged. Computational resources were provided by the e-INFRA CZ project (ID:90140), supported by the Ministry of Education, Youth and Sports of the Czech Republic.

APPENDIX: COMPUTATIONAL DETAILS

Several technical details omitted in the main text are documented here. First, is a derivation of the operators $\hat{\omega}_n(x, y, \phi, \partial_x)$ from the recurrence scheme (2.17). If $\hat{\omega}$, $\hat{Z}$, and γ (also included in A) are expanded in ϵ and the derivatives ∂_x commuted to the right, acting directly on p/A, the terms $\sim\epsilon^{n-1}$ give the equation of the form

$$\left[\partial_y(\partial_y - g\sin\phi) + q^2\partial_\phi^2\right]\hat{\omega}_n(x, y, \phi, \partial_x) = \hat{R}_n(x, y, \phi, \partial_x), \tag{A1}$$

fixing the operator $\hat{\omega}_n$. $\hat{R}_n = \sum_{k=0}^{n} R_{n,k}(x, y, \phi)\partial_x^k$ are composed of the lower order coefficients $\hat{\omega}_n$, $\hat{Z}_n$, γ_n', and their derivatives. In the zeroth order, Eq. (2.7) is recovered taking $\hat{R}_0 = 0$.

We expand $\hat{\omega}_n$ and the related $\hat{Z}_n$, $\hat{\gamma}_n'$, $\hat{R}_n$ also in g,

$$\hat{\omega}_n(x, y, \phi, \partial_x) = \sum_{k=0}^{\infty} g^k \hat{\omega}_{n,k}(x, y, \phi, \partial_x). \tag{A2}$$

For the coefficients, we obtain the chain of equations

$$\left[\partial_y^2 + q^2\partial_\phi^2\right]\hat{\omega}_{n,k} = \begin{cases} \sin\phi\ \partial_y\hat{\omega}_{n,k-1} + \hat{R}_{n,k}\ (\text{for } k > 0), \\ \hat{R}_{n,0}, \end{cases} \tag{A3}$$

which is solved readily after transformation to the complex plain, $z = qy + \mathrm{i}\phi$, $\bar{z} = qy - \mathrm{i}\phi$, simplifying Laplacian on the left-hand side to $4q^2\partial_z\partial_{\bar{z}}$. After integrations over z, $\bar{z}$ and returning back to y, ϕ, we have to provide periodicity in ϕ by eliminating the terms proportional to the powers of ϕ, adding the corresponding solutions $f(z) + \text{c.c.}$ of the Laplacian. Next, the BC

$$[\partial_y\hat{\omega}_{n,k} - \sin\phi\ \hat{\omega}_{n,k-1} \mp \hat{B}_{n,k}]_{y=\pm h(x)} = 0, \tag{A4}$$

where $\hat{B}_{n,k}$ is the coefficient at $\epsilon^n g^k$ of the operator

$$\hat{B} = \epsilon h' e^{-\gamma}(\partial_x - f\cos\phi)e^{\gamma}\hat{\omega}, \tag{A5}$$

coming from Eq. (2.4), and $\hat{\omega}_{n,-1} = 0$, are satisfied for any ϕ by adding the proper linear combination of e^{lz}, $e^{l\bar{z}}$, $l = -n-k, \ldots, n+k$. Finally, the constant is fixed to hold the normalization, $\int_{-h(x)}^{h(x)} dy \int_0^{2\pi} d\phi\ \hat{\omega}_{n,k}$ for any n, k except of $n = k = 0$.

Complexity of the expressions quickly grows for the higher n, k; we derived them by the computer algebra systems up to the terms $\sim\epsilon^3 g^0$ and $\epsilon^2 g^2$, giving the next order corrections to γ_1, γ_2, Eqs. (2.21), (2.22), depicted in Fig. 3. The asymptotics of these terms for the isotropic force $g = \sqrt{\epsilon} f$ in the leading order of $\sim f^2$ are then given by

$$\begin{aligned} \frac{\gamma_{a,3}}{f^2} &= \int \left[\frac{1}{q^3}\left(\frac{h'^5}{16h^2} - \frac{h'^3h''}{4h}\right) - \frac{1}{q^4}\left(\frac{h'^3h''}{4h^2} + \frac{h'h''^2}{4h}\right.\right. \\ &\quad \left. + \frac{h'^2h^{(3)}}{6h} + \frac{h'h^{(4)}}{12}\right) - \frac{1}{q^5}\left(\frac{15h'h''^2}{16h^2} + \frac{h'^2h^{(3)}}{h^2}\right. \\ &\quad \left.\left. - \frac{13h''h^{(3)}}{4h} - \frac{h'h^{(4)}}{h}\right) + \frac{1}{q^6}\left(\frac{11h'h^{(4)}}{16h^2} - \frac{h^{(5)}}{2h}\right)\right]dx \\ &= \int \left(\frac{h'h''(hh'' - 5h'^2)}{12q^4h^2} + \frac{3h'h''^2}{16q^5h^2} + \frac{3h'h^{(4)}}{16q^6h^2}\right)dx \\ &\quad - \frac{h'^4}{16q^3h} - \frac{1}{q^4}\left(\frac{h'^2h''}{6h} + \frac{h'h^{(3)}}{12} - \frac{h''^2}{24}\right) \\ &\quad + \frac{1}{q^5}\left(\frac{h'h^{(3)}}{h} + \frac{9h''^2}{8h}\right) - \frac{h^{(4)}}{2q^6h}; \end{aligned} \tag{A6}$$

the leading contribution to $\Delta\gamma$ coming from the formally unintegrable terms $\sim\epsilon^3/q^4 = \epsilon/\alpha^2$ corrects the shift of Eq. (3.2) with respect to the numerical data in Fig. 3.

Next, we extend the Stratonovich formula (3.3) for the spatial dependent $D(x)$ and give some notes on drawing of the fully dimensional stationary solution $\bar{\rho}_s(x, y)$ and the currents in Fig. 6. The generalized FJ equation (1.1) enables us to write the 1D stationary solution $p_s(x)$ as

$$\frac{p_s(x)}{A(x)} = \rho_0 - \int_0^x \frac{J\,dx'}{A(x')D(x')}. \tag{A7}$$

In a periodic channel, $h(x + L) = h(x)$, we set the integration constant ρ_0 to fix one particle per period L. We also require periodicity of the 1D stationary density $p_s(x) = p_s(x + L)$. Thus for a nonzero $\Delta\gamma = \gamma(x + L) - \gamma(x)$, $A(x)$ (unlike $A_0(x)$ and $D(x)$) is not periodic,

$$A(x + L) = A_0(x + L)e^{\gamma(x+L)} = A(x)e^{\Delta\gamma}. \tag{A8}$$

If it is applied in the condition of periodicity, we find

$$(1 - e^{-\Delta\gamma})\rho_0 = \int_0^L \frac{J\,dx'}{A(x')D(x')},$$

and after using Eq. (A8) and some algebra

$$\frac{p_s(x)}{A(x)} = \frac{J}{(e^{\Delta\gamma} - 1)}\int_{x-L}^{L} \frac{dx'}{A(x')D(x')}. \tag{A9}$$

Normalization $\int_0^L p_s(x)dx = 1$ gives Eq. (3.3).

Determining the stationary 1D density $p_s(x)$, we can reconstruct the corresponding 2D density by the backward mapping, Eq. (2.12). The net 2D stationary density $\bar{\rho}_s(x, y)$, plotted in Fig. 5 is its integral over ϕ,

$$\bar{\rho}_s(x, y) = e^{\gamma(x)}\int_0^{2\pi} d\phi\ \hat{\omega}(x, y, \phi, \partial_x)\frac{p_s(x)}{A(x)}. \tag{A10}$$

The components of polarization $\vec{P}$ are given by averaging $\cos\phi$ and $\sin\phi$ weighted by ρ over the orientation,

$$\begin{aligned} P_x(x, y) &= f e^{\gamma(x)}\int_0^{2\pi} \cos\phi\ d\phi\ \hat{\omega}(x, y, \phi, \partial_x)\frac{p_s(x)}{A(x)}, \\ P_y(x, y) &= f e^{\gamma(x)}\int_0^{2\pi} \sin\phi\ d\phi\ \hat{\omega}(x, y, \phi, \partial_x)\frac{p_s(x)}{A(x)}, \end{aligned} \tag{A11}$$

and the components of the stationary net current density, depicted as streamlines, are calculated according to

$$\begin{aligned} j_x(x, y) &= \int_0^{2\pi} d\phi\ (f\cos\phi - \partial_x)e^{\gamma(x)}\hat{\omega}(x, y, \phi, \partial_x)\frac{p_s(x)}{A(x)}, \\ j_y(x, y) &= \frac{e^{\gamma(x)}}{\epsilon}\int_0^{2\pi} d\phi\ (g\sin\phi - \partial_y)\hat{\omega}(x, y, \phi, \partial_x)\frac{p_s(x)}{A(x)}. \end{aligned} \tag{A12}$$

To get consistent results, we need to truncate the expansion of j_x and j_y in ϵ such that $\vec{\nabla}\cdot\vec{j} = 0$. Taking the terms up to ϵ^1, as done in Fig. 6, requires us also to express the operator $\hat{Z}_2$ within the recurrence scheme.

[1] P. Romanczuk, M. Bär, W. Ebeling, B. Lindner, and L. Schimansky-Geier, Eur. Phys. J. Spec. Top. **202**, 1 (2012).
[2] E. Fodor and M. C. Marchetti, Physica A **504**, 106 (2018).
[3] S. Ramaswamy, Annu. Rev. Condens. Matter Phys. **1**, 323 (2010).
[4] M. C. Marchetti, J. F. Joanny, S. Ramaswamy, T. B. Liverpool, J. Prost, M. Rao, and R. A. Simha, Rev. Mod. Phys. **85**, 1143 (2013).
[5] J. Prost, F. Jülicher, and J.-F. Joanny, Nat. Phys. **11**, 111 (2015).
[6] A. Walther and A. H. E. Müller, Soft Matter **4**, 663 (2008).
[7] A. Walther and A. H. E. Müller, Chem. Rev. **113**, 5194 (2013).
[8] C. Bechinger, R. Di Leonardo, H. Löwen, C. Reichhardt, G. Volpe, and G. Volpe, Rev. Mod. Phys. **88**, 045006 (2016).
[9] J. M. Rubi, Europhys. Lett. **127**, 10001 (2019).
[10] P. Galajda, J. Keymer, P. Chaikin, and R. Austin, J. Bacteriol. **189**, 8704 (2007).
[11] S. Elizabeth Hulme, W. R. DiLuzio, S. S. Shevkoplyas, L. Turner, M. Mayer, H. C. Berg, and G. M. Whitesides, Lab Chip **8**, 1888 (2008).
[12] G. Mahmud, C. J. Campbell, K. J. M. Bishop, Y. A. Komarova, O. Chaga, S. Soh, S. Huda, K. Kandere-Grzybowska, and B. A. Grzybowski, Nat. Phys. **5**, 606 (2009).
[13] G. Volpe, I. Buttinoni, D. Vogt, H.-J. Kümmerer, and C. Bechinger, Soft Matter **7**, 8810 (2011).
[14] A. Sokolov, M. M. Apodaca, B. A. Grzybowski, and I. S. Aranson, Proc. Natl. Acad. Sci. U.S.A. **107**, 969 (2010).
[15] A. Bricard, J.-B. Caussin, N. Desreumaux, O. Dauchot, and D. Bartolo, Nature (London) **503**, 95 (2013).
[16] R. Di Leonardo, L. Angelani, D. Dell'Arciprete, G. Ruocco, V. Iebba, S. Schippa, M. P. Conte, F. Mecarini, F. De Angelis, and E. Di Fabrizio, Proc. Natl. Acad. Sci. U.S.A. **107**, 1541 (2010).
[17] N. Koumakis, A. Lepore, C. Maggi, and R. Di Leonardo, Nat. Commun. **4**, 2588 (2013).
[18] L. Angelani, R. Di Leonardo, and G. Ruocco, Phys. Rev. Lett. **102**, 048104 (2009).
[19] P. K. Ghosh, V. R. Misko, F. Marchesoni, and F. Nori, Phys. Rev. Lett. **110**, 268301 (2013).
[20] P. K. Ghosh, P. Hänggi, F. Marchesoni, and F. Nori, Phys. Rev. E **89**, 062115 (2014).
[21] L. Angelani, A. Costanzo, and R. Di Leonardo, Europhys. Lett. **96**, 68002 (2011).
[22] N. Koumakis, C. Maggi, and R. Di Leonardo, Soft Matter **10**, 5695 (2014).
[23] B.-Q. Ai, Q.-Y. Chen, Y.-F. He, F.-G. Li, and W.-R. Zhong, Phys. Rev. E **88**, 062129 (2013).
[24] B.-Q. Ai, Y.-F. He, and W.-R. Zhong, J. Chem. Phys. **141**, 194111 (2014).
[25] C. J. O. Reichhardt and C. Reichhardt, Annu. Rev. Condens. Matter Phys. **8**, 51 (2017).
[26] M. B. Wan, C. J. Olson Reichhardt, Z. Nussinov, and C. Reichhardt, Phys. Rev. Lett. **101**, 018102 (2008).
[27] I. Berdakin, Y. Jeyaram, V. V. Moshchalkov, L. Venken, S. Dierckx, S. J. Vanderleyden, A. V. Silhanek, C. A. Condat, and V. I. Marconi, Phys. Rev. E **87**, 052702 (2013).
[28] K. Bisht and R. Marathe, Phys. Rev. E **101**, 042409 (2020).
[29] X. Ao, P. K. Ghosh, Y. Li, G. G. Schmid, P. Hänggi, and F. Marchesoni, Europhys. Lett. **109**, 10003 (2015).
[30] E. Yariv and O. Schnitzer, Phys. Rev. E **90**, 032115 (2014).
[31] P. Malgaretti and H. Stark, J. Chem. Phys. **146**, 174901 (2017).
[32] M. Sandoval and L. Dagdug, Phys. Rev. E **90**, 062711 (2014).
[33] A. M. Puertas, P. Malgaretti, and I. Pagonabarraga, J. Chem. Phys. **149**, 174908 (2018).
[34] U. M. B. Marconi, P. Malgaretti, and I. Pagonabarraga, J. Chem. Phys. **143**, 184501 (2015).
[35] L. Caprini, F. Cecconi, and U. Marini Bettolo Marconi, J. Chem. Phys. **150**, 144903 (2019).
[36] P. Kalinay, Phys. Rev. E **104**, 014608 (2021).
[37] P. Kalinay and F. Slanina, Phys. Rev. E **104**, 0 064115 (2021).
[38] P. Kalinay, Phys. Rev. E **106**, 044126 (2022).
[39] M. H. Jacobs, *Diffusion Processes* (Springer, New York, 1967).
[40] R. Zwanzig, J. Phys. Chem. **96**, 3926 (1992).
[41] D. Reguera and J. M. Rubí, Phys. Rev. E **64**, 061106 (2001).
[42] P. Kalinay and J. K. Percus, J. Chem. Phys. **122**, 204701 (2005).
[43] P. Kalinay and J. K. Percus, Phys. Rev. E **74**, 041203 (2006).
[44] S. Martens, G. Schmid, L. Schimansky-Geier, and P. Hänggi, Phys. Rev. E **83**, 051135 (2011); Chaos **21**, 047518 (2011).
[45] P. Kalinay, Phys. Rev. E **84**, 011118 (2011).
[46] P. Kalinay and J. K. Percus, Phys. Rev. E **83**, 031109 (2011).
[47] P. Kalinay and F. Slanina, J. Phys.: Condens. Matter **30**, 244002 (2018).
[48] A. M. Berezhkovskii, M. A. Pustovoit, and S. M. Bezrukov, J. Chem. Phys. **126**, 134706 (2007).
[49] I. Pineda, M.-V. Vazquez, A. M. Berezhkovskii, and L. Dagdug, J. Chem. Phys. **135**, 224101 (2011).
[50] S. Denisov, P. Hänggi, and J. L. Mateos, Am. J. Phys. **77**, 602 (2009).
[51] D. Cubero and F. Renzoni, Phys. Rev. Lett. **116**, 010602 (2016).
[52] R. L. Stratonovich, Radiotekh. Elektron. **3**, 497 (1958), in Russian.
[53] P. Reimann, C. Van den Broeck, H. Linke, P. Hänggi, J. M. Rubi, and A. Pérez-Madrid, Phys. Rev. E **65**, 031104 (2002).
[54] S. Lifson and J. L. Jackson, J. Chem. Phys. **36**, 2410 (1962).